IEEE Access
Multidisciplinary | Rapid Review | Open Access Journal

Received September 9, 2019, accepted September 26, 2019, date of publication October 3, 2019, date of current version October 17, 2019.

Digital Object Identifier 10.1109/ACCESS.2019.2945337

A Linearization Model of Turbofan Engine for Intelligent Analysis Towards Industrial Internet of Things

LINFENG GOU[1], XIANYI ZENG[1], ZHAOHUI WANG[3], GUANGJIE HAN[2,3], (Senior Member, IEEE), CHUAN LIN[3], (Student Member, IEEE), AND XU CHENG[1]

[1]School of Power and Energy, Northwestern Polytechnical University, Xi'an 710119, China
[2]College of Engineering, Nanjing Agricultural University, Nanjing 210095, China
[3]Key Laboratory for Ubiquitous Network and Service Software of Liaoning province, School of Software, Dalian University of Technology, Dalian 116024, China

Corresponding author: Guangjie Han (hanguangjie@gmail.com)

This work was mainly funded by the National Science and Technology Major Project under Grant 2017-V-0011-0062.

ABSTRACT Big data processing technologies, e.g., multi-sensor data fusion and cloud computing are being widely used in research, development, manufacturing, health monitoring and maintenance of aero-engines, driven by the ever-rapid development of intelligent manufacturing and Industrial Internet of Things (IIoT). This has promoted rapid development of the aircraft engine industry, increasing the aircraft engine safety, reliability and intelligence. At present, the aero-engine data computing and processing platform used in the industrial Internet of things is not complete, and the numerical calculation and control of aero-engine are inseparable from the linear model, while the existing aero-engine model linearization method is not accurate enough to quickly calculate the dynamic process parameters of the engine. Therefore, in this paper, we propose a linear model of turbofan engine for intelligent analysis in IIoT, with the aim to provide a new perspective for the analysis of engine dynamics. The construction of the proposed model includes three steps: First, a nonlinear mathematical model of a turbofan engine is established by adopting the component modeling approach. Then, numerous parameters of the turbofan engine components and their operating data are obtained by simulating various working conditions. Finally, based on the simulated data for the engine under these conditions, the model at the points during the dynamic process is linearized, such that a dynamic real-time linearized model of turbofan engine is obtained. Simulation results show that the proposed model can accurately depict the dynamic process of the turbofan engine and provide a valuable reference for designing the aero-engine control system and supporting intelligent analysis in IIoT.

INDEX TERMS Industrial Internet of Things, multi-sensor data fusion, cloud computing, turbofan engine, linearized model.

I. INTRODUCTION

Currently, although the civil aviation traffic and industry are booming and developing rapidly, aircraft flight accidents still occur frequently [1]. Meanwhile, aero-engines require strict reliability, safety, economic and maintenance guarantees, which creates challenges for their control systems [2]. That is to say, the demands of the aviation industry are increasing together with its challenges [3]. Nowadays, various kinds of Engine Health Monitoring (EHM) systems [4] are exist that can collect data from each component of aero-engine. For instance, in paper [5], Hanachi *et al.* surveyed state-of-the-art condition monitoring, diagnostic and prognostic techniques using performance parameters acquired from gas-path data that are mostly available from the operating systems of gas turbines. In [6], Yildirim *et al.* proposed Modern condition monitoring-based methods to reduce maintenance costs, increase aircraft safety, and reduce fuel consumption. As a result, enormous amounts of data pertaining to the engine are generated and transferred to the aero-engine control system for further processing [7].

In recent years, the development and application of Industrial Internet of Things (IIoT) [8]–[11] has promoted interconnection, sharing and intelligence for data processing of

The associate editor coordinating the review of this manuscript and approving it for publication was Chun-Wei Tsai.

the aero-engine. In [12], Hugh *et al.* introduces IIoT technology, which aims to integrate various collectors, sensors and controllers having the abilities of sensing and monitoring into the production and operation of the aero-engine industry. Furthermore, it adopts advanced computing techniques [13], e.g., cloud computing and fog computing to enable intelligent analysis and control for the aero-engine industry [14]–[16]. The IIoT-based aero-engine analysis architecture proposed in [17] mainly includes four layers, i.e., the perception layer, network layer, platform layer and application layer.

As mentioned above, an efficient model for aero-engine deployed at the platform layer of IIoT is indispensable for industrial analysis. Since the aero-engine is highly complex and has several non-linear features, designing an aero-engine model is a non-trivial task [18]. Therefore, devising a linear aero-engine model is an important research direction and objective toward achieving intelligent analysis in IIoT [19].

At present, the research on the linear model of engine mainly focuses on two aspects: 1) construction of a linear engine model; 2) improvement or optimization of an existing linear model. For instance, in [20], a linear model is established or modified on account of equilibrium and non-equilibrium states, respectively, such that the system transition state can be obtained. Based on this work, the authors in [21] propose an improved local linear model by introducing the parameters of Gaussian processing. Meanwhile, some recent work also establishes a linear model independent of dispatching to improve the integrated control of the turbofan engine [22], [23].

However, to support efficient/intelligent analysis for turbofan engine in IIoT especially in the presence of big industrial data, the following challenges have to be confronted and addressed: 1) the linear steady-state model based on small deviation mode cannot accurately describe the real working state of the turbofan engine [24]; 2) existing data processing capability of the aero-engine control system is limited [19]; 3) existing models cannot be adapted to the big data analysis in IIoT.

To address the aforementioned issues, we propose an accurate dynamic real-time analysis based linear model for turbofan engine which mainly contributes in the following aspects:

1 The analytical method we proposed is based on the model of component development, which is more universal and can be applied to analyze and calculate linear models for different types of aero-engines. The data obtained from turbofan engine can be used to describe turbofan engine accurately.
2 The nonlinear engine model can be linearized in real time based on the equilibrium point and dynamic point, which improves the operation efficiency and data utilization rate.
3 The linearized model established by our method can play a better role in IIoT.

The rest of this paper is organized as follows: A survey of related works is conducted in Sec. II. The system model is presented in Section. III. In Section. IV, some simulation and verification results are given to evaluate linearized model. Section. V concludes the paper and discusses the future directions of research.

II. RELATED WORK

In this section, we review existing research on aero-engine mode linearization and its application towards IIoT.

Recently, with the improvement of computer simulation technology and development of big data cloud computing technology [25], computer engine modeling is increasingly being used in research [26]. Meanwhile, aero-engine health management has developed rapidly. By analyzing and processing the collected data, the airborne health management system can monitor the working condition of the engine, further analyze the collected data, and realize the functions of fault diagnosis, trend analysis and life management of the engine. With the improvement of engine calculation method, the Internet of things in aero-engine industry is becoming complete.

Taking the example of a common mechanical, turbofan engine, that is widely used in civil aviation [27], an aero-engine can be seen as a complex aerothermodynamics system with multiple rotating components, multiple cavities, multi-coupling and strong nonlinearity. Its operating process involves many aspects such as gas dynamics, thermodynamics, chemistry and mechanics [28], [29]. The split multi-row turbofan engine is composed of intake components, i.e., fan and compressor, combustion component, i.e., combustion chamber, turbine components, i.e., turbine, exhaust components, i.e., nozzle and bypass and rotor components.

In order for an aero-engine to be stable under diverse environmental and operating conditions, it is necessary to control the complex and changeable working process of the engine [30] so that it can operate reliably and perform to the fullest its performance and benefit [31]. At the same time, a linear model of the aeroengine with real-time analysis [32] and calculation abilities is essential for the control system.

At present, engine modeling usually adopts component method. The basic concept of the component method is to establish a model based on the input and output relation of each component and the aerodynamic constraint relation between different components [33]. The engine model based on the component method can be theoretically accurate.

For instance, in [34], Wang *et al.* demonstrated that computer simulations can reduce the cost of research and development and make up for the lack of field testing. In [35], Chung *et al.* established an analytical linear model that can capture the engine dynamics during aggressive transient maneuvers. In [26], Popelka *et al.* obtained the output characteristics and mathematical model of the engine by solving nonlinear equations. In [36], Yang *et al.* obtained a linear model with acceptable accuracy by piecewise linearizing the working state of the engine. In the latest research [37], Yang *et al.* obtained the linear model of each component through the Taylor series expansion of these nonlinear expressions at the current working point, that is, the linearization of each

component is realized by the partial derivative of the output of each independent input. The introduction of partial derivatives further improves the accuracy of the model.

III. REAL-TIME LINEARIZATION METHOD BASED ON BIG DATA ANALYSIS

The linear model of engine is integrated from the linear model of components according to the actual structure of engine. The linear model of components can be freely combined into the state space model of any target engine. The analytical linearization method can be used to solve the linear model as long as the engine model is expressed in a suitable form [38]. The analytical linearization of the engine model proposed in this paper is realized through two steps. The first step is to make simplified assumptions for the nonlinear model of the engine and convert the engine description equation into an algebraic expression that can be analytically linearized. The second step is to obtain the linear model of the engine by Taylor expansion of these algebraic expressions. Fig. 1 shows the comparison between the traditional small perturbation method and the analytical linearization method.

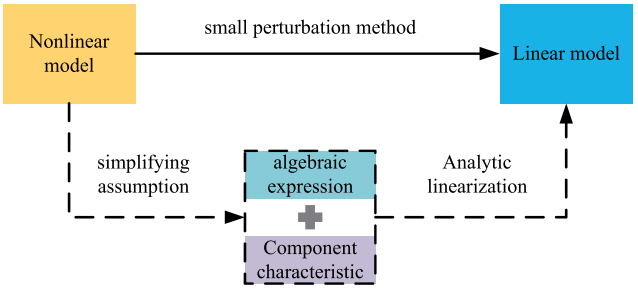

FIGURE 1. Two different linearization methods.

A. NONLINEAR MODEL OF TURBOFAN ENGINE USING COMPONENT METHOD

In this sub-section, we give the non-linear mathematical relations between input and output parameters of each component. Taking the components of a turbofan engine as a unit, the relationship between the input and output parameters of the components is completely expressed in the form of a mathematical function based on the internal characteristics of the components and the aerodynamic and thermodynamic processes.

The operating process of the split-row turbofan engine [39]: the air flows into the fan through the inlet deceleration and pressurization, and the fan's outlet airflow is divided into two parts. One part enters the outer culvert and expands through its nozzle to generate thrust, and the remaining airflow flows into a compressor for further compression [40]. Most of the outlet airflow from the compressor flows into the combustion chamber to participate in combustion, and a small part of the airflow is extracted to be used for aircraft air supply and cooling of turbines. The high-temperature and high-pressure gas produced by combustion expands in the turbine, and the generated power is used to drive the fan and compressor. Finally, the gas flow is discharged from the nozzles and thrust is generated. The numerical calculation process of a fractional turbofan engine is as TABLE 1.

TABLE 1. List of Symbols.

Symbol	Paraphrase
k_w	Flow loss factor
k_π	Pressure ratio loss factor
k_η	Efficiency loss factor
K	Loss factor
W_c	Flow rate
N_c	Power
H_u	The low calorific value of fuel oil
η_b	Combustion efficiency
H	Enthalpy
J	The moment of inertia of the rotor
τ	Output torque
FAR	Fuel to air Ratio
HP/LP	High/Low presser
C	Compressor
T	Turbine
Ma	Mach number

1) COMPRESSOR

The conversion speed ($n_{2,cor}$), conversion flow rate ($W'_{25,cor}$), pressure ratio (π'_{CH}) and efficiency (η'_{CH}) of HP compressor are given as follows:

$$\left.\begin{aligned} n_{2,cor} &= n_2\sqrt{\frac{T_0}{T_{t25}}} \\ W'_{25,cor} &= f_1(n_{2,cor}, R_{CH}) \\ \pi'_{CH} &= f_2(n_{2,cor}, R_{CH}) \\ \eta'_{CH} &= f_3(n_{2,cor}, R_{CH}) \\ W_{25,cor} &= k_{WCH} W'_{25,cor} \frac{P_{t25}}{P_0}\sqrt{\frac{T_0}{T_{t25}}} \\ \pi_{CH} &= k_{\pi CH}(\pi'_{CH} - 1) + 1 \\ \eta_{CH} &= k_{\eta CH}\eta'_{Ch} \end{aligned}\right\}. \tag{1}$$

Total outlet pressure of HP compressor

$$P_{t3} = \pi_{CH} P_{t25}. \tag{2}$$

and the enthalpy change of compressor compression process is

$$H_3 = \frac{H_{3i} - H_{25}}{\eta_{ch}} + H_{25}. \tag{3}$$

Using the inlet parameters of HP compressor T_{t25}, P_{t25}, H_{25}, S_{25} and interpolated π_{CH}, η_{CH}, Export parameters can be calculated further T_3, H_3 and S_3.

The power required for all inlet airflows to be compressed from the inlet state to the outlet state

$$N_T = W_{25}(H_{25} - H_3). \tag{4}$$

The total pressure and enthalpy of the induced air flow in the HP compressor are as follows:

$$\left.\begin{aligned} \pi_{tc} &= P_{t25} + P_{t3} - P_{t25} \\ H_{CH} &= H_{25} + H_3 - H_{25} \end{aligned}\right\}. \tag{5}$$

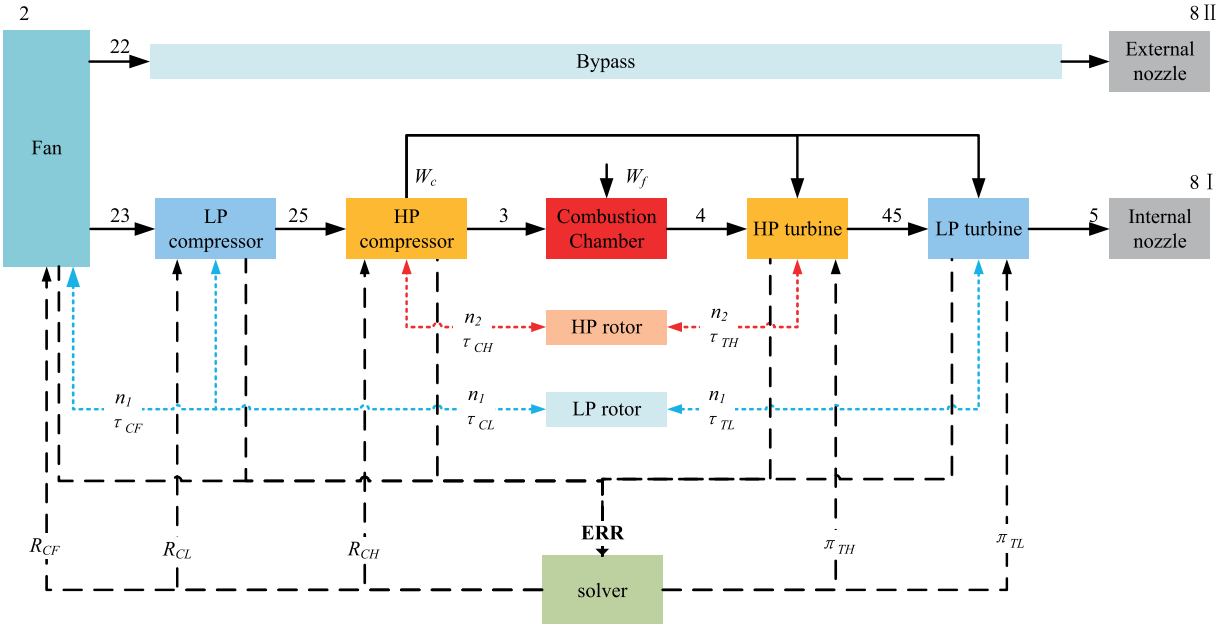

FIGURE 2. Schematic diagram of numerical calculation of Separate exhaust turbofan engine.

The output power (N_c) and torque (τ_{CH}) of HP compressor:

$$\left.\begin{aligned} N_c &= W_c(H_{25} - H_{CH}) \\ N_{CH} &= N_T + N_c - W_c(H_{25} - H_3) \\ \tau_{CH} &= (\frac{60}{2\pi})\frac{N_{CH}}{n_2} \end{aligned}\right\}. \tag{6}$$

2) COMBUSTOR CHAMBER

Combustor outlet flow (W_4), total pressure (P_{tout}) and fuel to gas ratio (FAR) are calculated as follows:

$$\left.\begin{aligned} W_4 &= W_3 + W_f \\ P_{tout} &= (1-K)P_{tin} \\ FAR_4 &= \frac{W_3 FAR_3 + W_f}{W_3(1 - FAR_3)} \end{aligned}\right\}. \tag{7}$$

According to the combustion chamber energy conservation equation

$$(W_3 + W_f)H_4 + W3H_3 + W_f H_u \eta_b \tag{8}$$

where H_4 is low calorific value of fuel; η_b is combustion efficiency of combustion chamber;

3) TURBINE

The exit enthalpy (H_4), flow rate (W_{45}) and fuel to gas ratio (FAR_{45}) of HP turbine are given as

$$\left.\begin{aligned} H_4 &= \frac{W_3 H_3 + W_f H_u \eta_u}{W_3 + W_f} \\ W_{45} &= W_{4a} = W_4 + W?a?acH \\ FAR_{45} &= \frac{\frac{W_4}{1+FAR_4}FAR_4 + \frac{W_{cH}}{1+FAR_{cH}}FAR_{cH}}{\frac{W_4}{1+FAR_4} + \frac{W_cH}{1+FAR_{cH}}} \end{aligned}\right\}. \tag{9}$$

where W_{4a} is air flow after mixing; FAR_{cH} is fuel to air Ratio of high-pressure turbine cooling airflow.

Based on the conservation of energy before and after mixing, the following expression can be obtained:

$$W_{cH}H_{cH} + W_4 H_4 = W_{4a}H_{4a}. \tag{10}$$

where H4a is enthalpy of the mixed flow.

The converted speed of HP turbine is given by the following expression:

$$n_{2,cor} = n_2\sqrt{\frac{T_0}{T_{t4}}}. \tag{11}$$

The reduced flow under current conditions and the corresponding efficiency value are given as

$$\left.\begin{aligned} W'_{4,cor} &= g_1(n_{2,cor}, \pi_{TH}) \\ \eta'_{TH} &= g_2(n_{2,cor}, \pi_{TH}) \\ W_{4,cor} &= k_{WTH}W'_{4,cor} \\ \eta_{TH} &= k_{\eta TH}\eta'_{TH} \end{aligned}\right\}. \tag{12}$$

The total outlet pressure (P_{t45}) and actual enthalpy (H_{45}) at the outlet of high-pressure turbines are

$$\left.\begin{aligned} P_{t45} &= \frac{P_{t4}}{\pi_{TH}} \\ H_{45} &= H_{4a} - \eta_{TH}(H_{4a} - H_{45i}) \end{aligned}\right\}. \tag{13}$$

The output power (N_{TH}) and torque (τ_{TH}) of the high-pressure turbine are given as follows:

$$\left.\begin{aligned} N_{TH} &= W_{4a}(H_{4a} - H_{45}) \\ \tau_{TH} &= (\frac{60}{2\pi})\frac{N_{TH}}{n_2} \end{aligned}\right\}. \tag{14}$$

4) EXHAUST NOZZLE

The outlet flow state is expressed by the pressure ratio, the critical pressure ratio and the true pressure ratio of the nozzle are calculated as follows:

$$\left.\begin{aligned}\beta_c r &= \frac{P_{ecr}}{P_t} = \left(\frac{2}{k+1}\right)^{\frac{k}{k-1}} \\ \beta &= \frac{P_b}{P_t 5}\end{aligned}\right\}. \tag{15}$$

where P_t is total pressure at nozzle inlet; P_b is ambient pressure at nozzle outlet.

when the airflow is in a critical or supercritical state, the Mach number of the outlet flow equal to 1, i.e., $M_a = 1$.

The outlet static pressure (P_{8I}), velocity (v_{8I}) and flow flow (W_{8I}) of the nozzle and the thrust of the engine (F_{8I}) can be calculated from the following formula

$$\left.\begin{aligned}P_{8I} &= P_{t5}\beta_{cr} \\ v_{8I} &= v_{cr} = \sqrt{\frac{2kRT_{t5}}{k+1}} \\ W_{8I} &= K\frac{P_{t5}}{\sqrt{T_{t5}}}A_{8I} \\ F_{8I} &= W_{8I} + (P_{8I} - P_b)A_{8I}\end{aligned}\right\}. \tag{16}$$

when the airflow is in a subcritical state, the static pressure at the outlet of the nozzle is equal to the ambient pressure, i.e., $P_{8I} = P_b$.

The relationship between different parameters is given below:

$$\left.\begin{aligned}v_{8I} &= \sqrt{\frac{2k}{k-1}RT_{t5}\left[1 - \left(\frac{P_b}{P_{t5}}\right)^{\frac{k-1}{k}}\right]} \\ \rho_{8I} &= \frac{P_{t5}}{RT_{t5}}\left(\frac{P_{t5}}{P_b}\right)^{-\frac{1}{k}} \\ W_{8I} &= \rho_{8I}A_{8I}v_{8I} \\ F_{8I} &= W_{8I}v_{8I}\end{aligned}\right\}. \tag{17}$$

Once the parameters corresponding to the four parts of the engine are calculated, the complete mathematical model of the engine can be obtained according to the connection relation and balance equation between the different parts, as shown in Fig. 2.

B. LINEARIZATION OF NONLINEAR MODELS

Linearization means that the nonlinear relation of the system is approximated by linear expression at the operating point of the system [41]. The stronger the nonlinearity of the system, the smaller the approximate range of linearization. The general condition of linearization is that the system function is continuous in the linearized region and the system runs in the small range of the target operating point, that is, in the confidence range of linearization.

The improved Newton-Rapson method [42] utilized in this paper uses an iterative factor to correct the derivative of the output with respect to the input and guide the search direction of the optimal solution of the non-linear equations.

Given the following nonlinear equations

$$\begin{cases} f_1(x_1, x_2, \cdots, x_n) = 0 \\ f_2(x_1, x_2, \cdots, x_n) = 0 \\ f_n(x_1, x_2, \cdots, x_n) = 0 \end{cases}. \tag{18}$$

The iteration number is represented by k and ranges from 0 to n. Other parameters used in the above equations are given as

$$\begin{cases} x_k + 1 = x_k - \|J_k\|^{-1}e_k, & \|J_k\|^{-1} \le M \\ x_k + 1 = x_k - K_s\|J_k\|^{-1}e_k, & \|J_k\|^{-1} > M \end{cases}. \tag{19}$$

Iterative factors K_s is used to modify the derivative of the output to the input to guide the search direction of the optimal solution of the equation. When dealing with nonlinear equations, the same principle is used to determine the change direction of the respective variables, where

$$X_k = [x_1^{(k)} x_2^{(k)} x_3^{(k)}]^T. \tag{20}$$

$$e_k = [e_1^{(k)} e_2^{(k)} e_3^{(k)}]^T. \tag{21}$$

$$\begin{aligned} J_k &= \begin{bmatrix} \frac{\partial f_1}{\partial x_1} & \frac{\partial f_1}{\partial x_2} & \cdots & \frac{\partial f_1}{\partial x_n} \\ \frac{\partial f_2}{\partial x_1} & \frac{\partial f_2}{\partial x_2} & \cdots & \frac{\partial f_2}{\partial x_n} \\ \vdots & \vdots & \ddots & \vdots \\ \frac{\partial f_n}{\partial x_1} & \frac{\partial f_n}{\partial x_2} & \cdots & \frac{\partial f_n}{\partial x_n} \end{bmatrix} \\ &\approx \begin{bmatrix} \frac{\Delta f_1}{\Delta x_1} & \frac{\Delta f_1}{\Delta x_2} & \cdots & \frac{\Delta f_1}{\Delta x_n} \\ \frac{\Delta f_2}{\Delta x_1} & \frac{\Delta f_2}{\Delta x_2} & \cdots & \frac{\Delta f_2}{\Delta x_n} \\ \vdots & \vdots & \ddots & \vdots \\ \frac{\Delta f_n}{\Delta x_1} & \frac{\Delta f_n}{\Delta x_2} & \cdots & \frac{\Delta f_n}{\Delta x_n} \end{bmatrix}. \end{aligned} \tag{22}$$

For the nonlinear model of the engine mentioned above, the system state and output at any working (x_0, z_0, u_0) of the nonlinear system can be expressed as

$$\begin{cases} \dot{x}_0 = f(x_0, z_0, u_0) \\ \dot{z}_0 = m(x_0, z_0, u_0) = 0. \\ y_0 = g(x_0, z_0, u_0) \end{cases} \tag{23}$$

The dynamic function and the function of intermediate variables are expanded with Taylor series near the currently selected working point, and the higher order terms are omitted. The following expression can be obtained

$$\begin{aligned} &f'(x', z', u') \\ &= f(x_0 + \Delta x, z_0 + \Delta y, u_0 + \Delta u) \\ &\approx f(x_0, z_0, u_0) + \frac{\partial f}{\partial x}|_0\Delta x + \frac{\partial f}{\partial z}|_0\Delta z + \frac{\partial f}{\partial u}|_0\Delta u \\ &= f(x_0, z_0, u_0) + A'\Delta x + F\Delta z + B'\Delta u. \end{aligned} \tag{24}$$

$$
\begin{aligned}
&m(x', z', u') \\
&\quad = m(x_0 + \Delta x, z_0 + \Delta y, u_0 + \Delta u) \\
&\quad \approx m(x_0, z_0, u_0) + \frac{\partial m}{\partial x}|_0 \Delta x + \frac{\partial m}{\partial z}|_0 \Delta z + \frac{\partial m}{\partial u}|_0 \Delta u \\
&\quad = m(x_0, z_0, u_0) + M'\Delta x + K\Delta z + L'\Delta u. \qquad (25)
\end{aligned}
$$

where $m(x, y, z) = 0$, therefore, the expansion of the function of the intermediate variable can be expressed as $M \bigtriangleup x + K \bigtriangleup z + L \bigtriangleup u = 0$, i. e.

$$\Delta z = -K^{-1}M'\Delta x - K^{-1}L'\Delta u. \qquad (26)$$

Simplified expansion

$$
\begin{aligned}
f(x', z', u') &\approx f(x_0, z_0, u_0) + (A' - FK^{-1}M)\Delta x \\
&\quad + (B' - FK^{-1}L)\Delta u \\
&= f(x_0, z_0, u_0) + A\Delta x + B\Delta u. \qquad (27) \\
f'(x', z', u') &- f(x_0, z_0, u_0) \\
&= \Delta\dot{x} = A\Delta x + B\Delta u. \qquad (28)
\end{aligned}
$$

The linearization of the nonlinear engine model gives parameters to describe the linear model. In this paper, various components of the system are considered as part of a simple static system, and we will be able to achieve the linearization of each component using the partial derivative of the output with respect to independent input of each component [43].

Fig. 3 is a schematic diagram of the linearization process. Linearization of working point (x_0, z_0, u_0) will generate an effective region. A more accurate output estimation can be obtained by calculating point (x', z', u') in the region with the linear model obtained from this point. The arrow in the Figure represents the value of the current point state function, and the curve represents the working track of the system.

The Taylor series expansion of the output function to the working point (x_0, z_0, u_0) in the effective region can be expressed by the following formula, and the higher order can also be omitted, as follows

$$
\begin{aligned}
&g(x', z', u') \\
&\quad = g(x_0 + \Delta x, z_0 + \Delta y, u_0 + \Delta u) \\
&\quad \approx g(x_0, z_0, u_0) + \frac{\partial g}{\partial x}|_0 \Delta x + \frac{\partial g}{\partial z}|_0 \Delta z + \frac{\partial g}{\partial u}|_0 \Delta u \\
&\quad = g(x_0, z_0, u_0) + C'\Delta x + E\Delta z + D'\Delta u \\
&\quad = g(x_0, z_0, u_0) + (C' - EK^{-1}M)\Delta x \\
&\qquad + (D' - EK^{-1}L)\Delta u \\
&\quad = g(x_0, z_0, u_0) + C\Delta x + D\Delta u. \qquad (29) \\
&g'(x', z', u') - g(x_0, z_0, u_0) \\
&\quad = \Delta y = C\Delta x + D\Delta u. \qquad (30)
\end{aligned}
$$

The state space equation of the nonlinear system can be obtained

$$
\begin{cases}
\Delta\dot{x} = A\Delta x + B\Delta u \\
\Delta y = C\Delta x + D\Delta u.
\end{cases} \qquad (31)
$$

The above method linearizes the dynamic points along the working track. Compared with the traditional steady-state linearization method, a more consistent linear model can be obtained, which gives a more accurate estimation of the dynamic process, as shown in Fig. 4. In addition, this real-time linearization scheme for each dynamic working point also avoids the problems faced by the scheduling piecewise linear model.

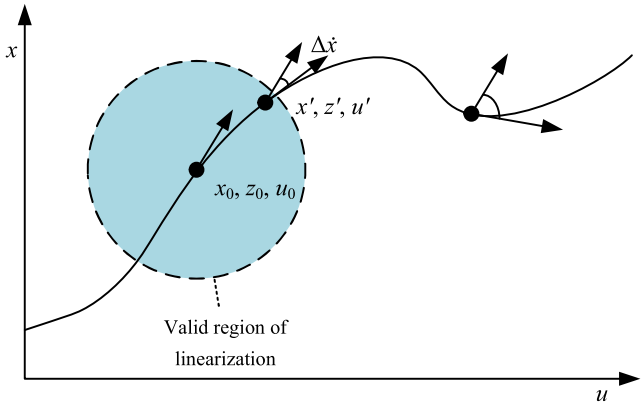

FIGURE 3. Diagram of the linearization process.

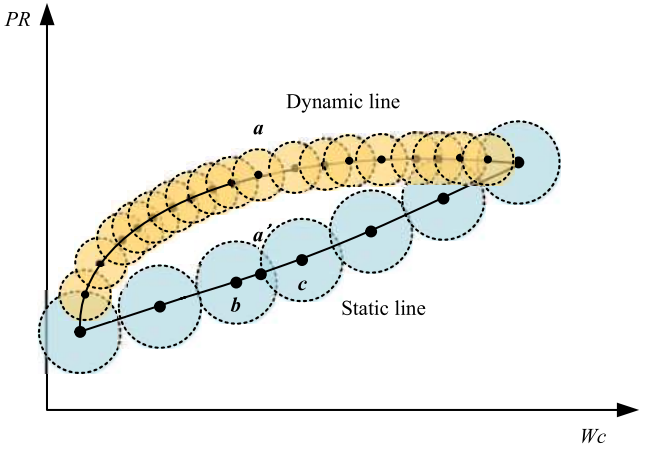

FIGURE 4. Linearization diagram of dynamic operating point.

The application of steady-state and dynamic calculations of the nonlinear engine model is based on the state change of the transmission components, i.e., whether the power on the rotor is balanced or not.

Dynamic calculations are used to obtain the state parameters of the engine during the transition from one steady-state to another. In these calculations, not only the rotor dynamics principle between the rotors should be complied with, but also the constraints of the common working equations between the components should be followed, so that the calculation results can be consistent with the actual working state of the engine.

In fact, not only the influence of rotor dynamics should be taken into account when establishing a high-precision nonlinear engine model, but also the cavity and heat transfer dynamics of high-temperature components involved should be taken into account.

During the functioning of the engine, ignoring the mechanical efficiency, the rotor motion equation used to calculate the rotor acceleration is as follows:

$$\begin{aligned} \tau_C + \tau_T &= J\frac{d\varpi}{dt} = J\frac{dn}{dt}\frac{2\pi}{60} \\ \frac{dn}{dt} &= \frac{60}{2}\frac{(\tau_C + \tau_T)}{J}. \end{aligned} \tag{32}$$

In this paper, only second-order rotor dynamics are considered in the modeling process, and the effects of volume and heat transfer dynamics are ignored.

For the general nonlinear system, x is the state, u is the input, y is the output of the system, z is the intermediate variable of the system, the m is the intermediate variable function, the g represents the output function of the system.

$$\begin{cases} \dot{x} = f(x, z, u) \\ \dot{z} = m(x, z, u) \\ y = g((x, z, u). \end{cases} \tag{33}$$

In the engine model considered in this paper, x refers to the rotor dynamic parameters of the engine, and z represents the volumetric dynamic parameters. As the volumetric dynamics are ignored, the flow, temperature and pressure parameters involved in each component of the engine are the same at the inlet and outlet. This leads to

$$\dot{z} = m(x, z, u) = 0. \tag{34}$$

As a result, the nonlinear model of the engine can be expressed as

$$\begin{cases} \dot{x} = f(x, z, u) \\ \dot{z} = m(x, z, u) = 0\ . \\ y = g((x, z, u) \end{cases} \tag{35}$$

After the linear model of each component is established, the overall linear model of the turbofan engine can be obtained. For this purpose, the structure of the exhaust turbofan engine is matched to each component by selecting appropriate input, output and intermediate state parameters. The linear coefficient matrix of each component is connected in series based on the structure of the engine. The linear model of the system is shown in Fig. 5.

The specific form of the linear state space model is as follows:

$$\begin{cases} \Delta\dot{x} = A\Delta x + B\Delta u + R\Delta w \\ \Delta y = C\Delta x + D\Delta u + S\Delta w. \end{cases} \tag{36}$$

With n_1, n_2 as dynamic models of the engine, the complete description of its input and output variables can be written as

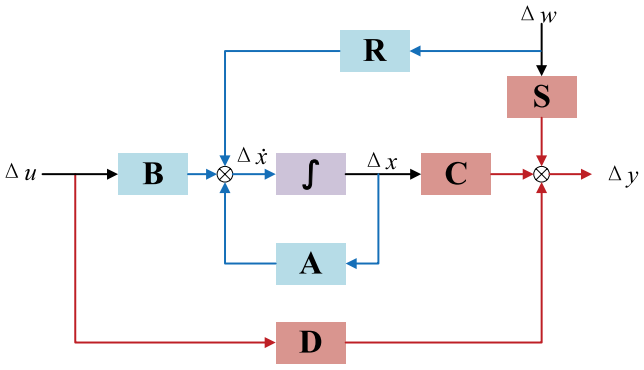

FIGURE 5. Linear model of the system.

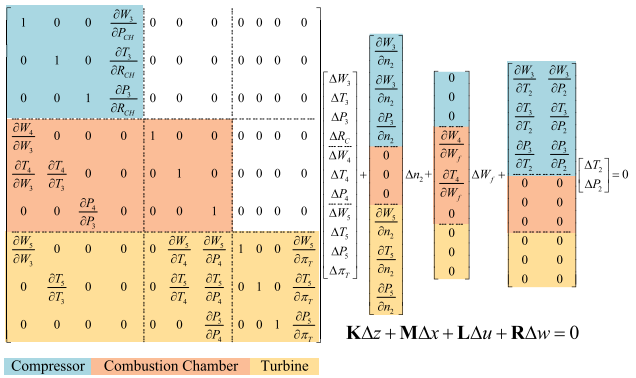

FIGURE 6. The core machine component model joint matrix.

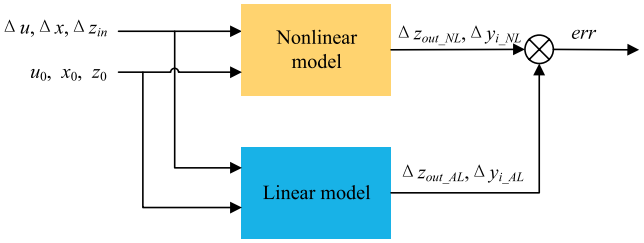

FIGURE 7. Accuracy verification schematic of Linear model.

follows:

$$u = \begin{bmatrix} w_f \\ A_{8I} \end{bmatrix} x = \begin{bmatrix} n_1 \\ n_2 \end{bmatrix} w = \begin{bmatrix} P_{t2} \\ T_{t2} \end{bmatrix} y = \begin{bmatrix} x \\ z \\ y' \end{bmatrix}. \tag{37}$$

$$y'_{(9\times1)} = [\tau_{CF}\,\tau_{CL}\,\tau_{CH}\,\tau_{TH}\,\tau_{TL}\,\nu_{8I}\,F_{8I}\,\nu_{8II}\,F_{8II}]^T. \tag{38}$$

$$\begin{aligned} z^T_{(26\times1)} = [&W_2 W_{23} T_{t23} P_{t23} R_{CF} \\ &W_{25} T_{t25} P_{t25} R_{CL} W_3 T_{t3} P_{t3} \\ &R_{CH} W_4 T_{t4} P_{t4} W_{45} P_{t45} \\ &\pi_{TH} W_5 T_{t5} P_{t5} \pi_{TL} W_{8I} W_{8II}]. \end{aligned} \tag{39}$$

The output vector of the system is composed of system state, i.e., n_1 and n_2, component parameters, i.e., N_c, T^* and P^*, linkage parameters represented by τ and performance parameters, i.e., F_g and V_9. For convenience, the out-

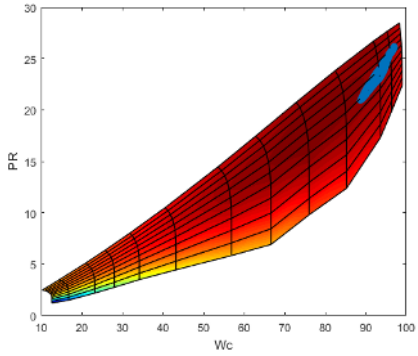

(a) HPC

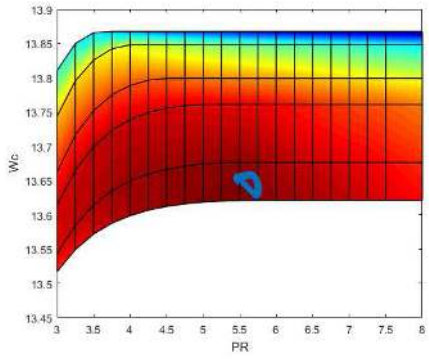

(b) HPT

FIGURE 8. The variation of engine state on the component characteristic diagram in transition state. (a) HPC. (a) HPT.

put parameters of the iterative solver, such as compressor R-line and turbine drop ratio data, are added into component parameters to jointly form the output vector of the system. Based on the composition of input/output and intermediate parameters, the linear coefficient matrix of each component can be combined to give the following form:

$$K_{(n\times n)}\Delta z_{(n\times l)}+M_{(n\times m)}\Delta x_{(m\times l)}+L_{(n\times m)}\Delta u_{(m\times l)}=0. \quad (40)$$

As the elements of the K matrix are independent of one another, the matrix is invertible. In the process of component combination, a large number of elements of the matrix K will be zero due to lack of correlation between different components. Based on this characteristic, the algorithm of matrix operation can be optimized to improve the speed of the state space model of the whole machine.

The component parameter vector Δz in (40) can be represented by system input and system state as follows:

$$\Delta z=-K^{-1}(L\Delta u+M\Delta x). \quad (41)$$

The torque and performance parameter vector $\bigtriangleup y'$ can also be integrated into component parameter vector $\bigtriangleup z$. However, to reduce the dimensions of K, improve the operation speed of the matrix and facilitate the solution of the system state space model, $\bigtriangleup y'$ is listed separately as

$$\begin{aligned}\Delta y' &= E\Delta z+F\Delta u+G\Delta x\\ &=(-EK^{-1}M+G)\Delta x+(-EK^{-1}+F)\Delta u. \quad (42)\end{aligned}$$

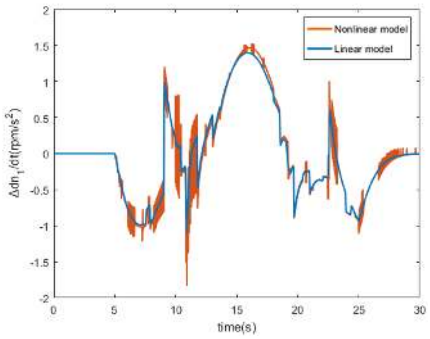

(a) Change of LP rotor acceleration increment

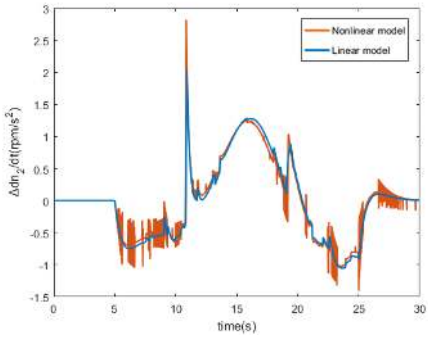

(b) Change of HP rotor acceleration increment

FIGURE 9. Dynamic variation of rotor in transition state.

After combining with the dynamic equation of the engine rotor, the state equation of the whole engine and output equation of the system can be written as

$$\begin{aligned}\Delta\dot{x} &= P\Delta y'\\ &=(-PEK^{-1}M+PG)\Delta x\\ &\quad+(-PEK^{-1}L+PF)\Delta u\\ &=A\Delta x+B\Delta u.\\ \Delta y &= C\Delta x+D\Delta u. \quad (43)\end{aligned}$$

$$\begin{cases}\Delta\dot{x}=A\Delta x+B\Delta u\\ \Delta y=C\Delta x+D\Delta u.\end{cases} \quad (44)$$

Fig. 6 shows an example matrix of a turbofan core engine [44]. For the ease of understanding, equations of all the components are integrated into the matrix K based on the order of engine structure. Due to the universality of this linearization method, a component equation can be included in K based on the specific structure of the target engine to obtain a new linear engine model. Each colored block in the figure represents a component, and the last block is reserved for storing the continuous flow equation.

IV. SIMULATION AND VERIFICATION

In this paper, a two-axis split turbofan engine model in the pneumatic system modeling and analysis toolbox (T-MATS) [45] compiled based on MATLAB/Simulink environment was selected to verify and evaluate the linearized model based on two linearized analysis methods.

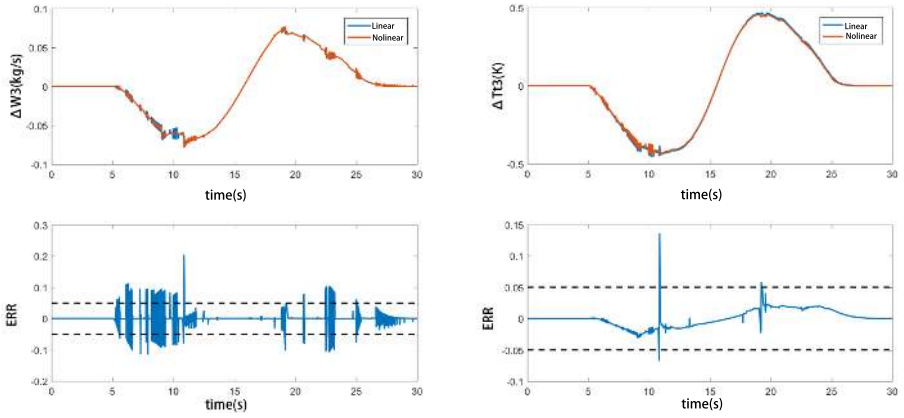

(a) W_3 (b) T_{t3}

FIGURE 10. Comparison of compressor component parameters.

Two types of verification of the linear model are carried out: steady-state verification and dynamic process verification. The accuracy of the linear model is evaluated by calculating the difference between the response of the nonlinear model and the response estimated from the linear model, as shown in the Fig. 7.

To avoid excessive error fluctuations caused by the incremental form of nonlinear response, which can render the error analysis meaningless, the maximum variation of nonlinear model response in the simulation process is used to normalize and calculate the final error [46], as shown below

$$ERR = \frac{\Delta y_{AL} - \Delta y_{NL}}{\Delta y_{NLmax}}. \tag{45}$$

A. DYNAMIC VALIDATION

Dynamic accuracy analyzes the deviation between the linear and non-linear models in the transition state. The engine is put under a large range of acceleration and deceleration to obtain the transition state, so that the state of the engine in the characteristic diagram changes over a large span.

Taking high-pressure compressor and high-pressure turbine as an example, under the given oil supply curve, the trace lines of the nonlinear model on the characteristics of the engine rotating components are shown in Fig. 8.

It is obvious from the figure that the steady-state point linearization method can only fit a limited number of points on the dynamic trajectory. It is obvious that the real-time dynamic linearization method proposed in this paper is superior to the steady-state point linearization method.

The simulation results of dynamic verification using a large range of transition states are shown in Fig. 9. The change in acceleration increment is the output of the state equation of the linear model of the engine. Where high-pressure and low-pressure rotor speed n_1, n_2 are two state variables of the selected model, and the fuel flow W_f is the input variable.

The simulation results show that the linear model can track the nonlinear model well under the same fuel input and speed changes, which proves the dynamic accuracy of the linearization method proposed in this paper, and can quickly fit the nonlinear model under dynamic conditions to track the real state of the engine in real time.

TABLE 2. The steady-state error in $H = 0$, $M_a = 0$.

	$W_f(kg/s)$	$n_1(rpm)$	$n_2(rpm)$	LP $error$	HP $error$
1	0.27216	2669.125	6666.020	0.0034	0.0019
2	0.31752	2789.850	6765.991	0.0021	0.0224
3	0.36288	2901.320	6856.176	0.0102	0.0092
4	0.40824	2999.701	6938.191	0.0201	0.0045
5	0.45360	3090.144	7012.782	0.0004	0.0086
6	0.49896	3167.525	7079.330	0.0005	0.0804
7	0.54432	3235.881	7160.294	0.0200	0.0727
8	0.58968	3300.929	7238.733	0.0353	0.0022
9	0.63504	3360.746	7315.372	0.0205	0.0159
10	0.68040	3420.198	7386.443	0.0068	0.0880

B. STEADY-STATE VERIFICATION

Steady-state accuracy analyzes the deviation between linear and nonlinear models when the former model transitions from the original steady-state point to the new steady-state point. This process generally uses the small perturbation method, which tests if the linear model, after being disturbed around a small range near the original steady-state point, gives results that are consistent with those of the non-linear model. We applied a step of $\pm 0.5s$ to the low-pressure rotor speed at the selected steady-state operating point 1. By referring to formula (45), we calculated the component output parameter changes and the errors of the linear model compared with the nonlinear model. The simulation results are shown in Fig. 10.

Simulation results show that except for the flow rate, the overall error can be defined within 5%, where the error of temperature, pressure and torque can be defined within 1% except for the step point, and the error at the step point is no more than 10%, indicating that the linear model has a high accuracy under the step input with a small range.

Select 10 different steady-state operating points of the engine under the condition of $H = 0$, $M_a = 0$,

the steady-state errors of the high pressure and low pressure rotor speed under different steady-state conditions were obtained, and the results are shown in TABLE 2.

It can be seen from the table that at the 10 operating points, the steady-state error is very small. Therefore, this method can fully reflect the calculation mechanism of the model and improve the efficiency of the model.

V. CONCLUSION

In this paper, we have proposed a linear model of the turbofan engine to enable intelligent analysis towards Industrial Internet of Things. Notably, the component method is adopted to address the problem of accurate engine modeling. For the dynamic process of engine, we propose an analytical method to carry out real-time linearization analysis and calculation at the dynamic point of engine. Compared with the current methods for constructing the linear model, the advantages of our proposal are as follows: the analytical linearization method based on component modeling can reflect the physical principle of the working process of the system, and can quickly fit the real process of turbofan engine, with high operating efficiency and flexible modification; compared with the traditional steady-state model, we add more accurate description of the dynamic process; the proposed method can be more easily applied to the industrial Internet of things by taking the EHM detection platform as the application carrier.

Possible future work that can be derived from this work is to make the method be more universal for different types of aero-engines by comprehensively analyzing and integrating the input/output data and many intermediate variables of engines. In addition, the analytical linear model can be improved to combine with some other factors, e.g., the engine health degradation, such that the engine degradation characteristics can be acquired and the applicability of the proposed method can be increased, leading to a more perfect IIoT system especially for the aero-engines.

REFERENCES

[1] G. Dillingham, "Aviation safety: Proposals to enhance aircraft tracking and flight data recovery may aid accident investigation, but challenges remain," *Fisheries Oceanogr.*, vol. 24, no. 4, pp. 325–334, Apr. 2015.

[2] G. Srinivas, K. Raghunandana, and B. S. Shenoy, "Recent developments in turbomachinery component materials and manufacturing challenges for aero engine applications," in *Proc. IOP Conf., Mater. Sci. Eng.*, Wuhan, China, Feb. 2018, vol. 314, no. 1, Art. no. 012012.

[3] J. Skorupski, "The risk of an air accident as a result of a serious incident of the hybrid type," *Rel. Eng. Syst. Saf.*, vol. 140, pp. 37–52, Aug. 2015.

[4] C. Kong, "Review on advanced health monitoring methods for aero gas turbines using model based methods and artificial intelligent methods," *Int. J. Aeronaut. Space Sci.*, vol. 15, no. 2, pp. 123–137, Jun. 2014.

[5] H. Hanachi, C. Mechefske, J. Liu, A. Banerjee, and Y. Chen, "Performance-based gas turbine health monitoring, diagnostics, and prognostics: A survey," *IEEE Trans. Rel.*, vol. 67, no. 3, pp. 1340–1363, May 2018.

[6] M. T. Yildirim and B. Kurt, "Aircraft gas turbine engine health monitoring system by real flight data," *Int. J. Aerosp. Eng.*, vol. 2018, no. 10, Dec. 2017, Art. no. 9570873.

[7] D. Zhang, C. C. Chan, and G. Y. Zhou, "Enabling industrial Internet of Things (IIoT) towards an emerging smart energy system," *Global Energy Interconnection*, vol. 1, no. 1, pp. 39–47, Jan. 2018.

[8] A. Buda, K. Främling, J. Borgman, M. Madhikermi, S. Mirzaeifar, and S. Kubler, "Data supply chain in Industrial Internet," in *Proc. IEEE World Conf. Factory Commun. Syst. (WFCS)*, May 2015, pp. 1–7. doi: 10.1109/WFCS.2015.7160559.

[9] G. Han, H. Guan, J. Wu, S. Chan, L. Shu, and W. Zhang, "An uneven cluster-based mobile charging algorithm for wireless rechargeable sensor networks," *IEEE Syst. J.*, to be published. doi: 10.1109/JSYST.2018.2879084.

[10] G. Han, J. Wu, H. Wang, M. Guizani, J. A. Ansere, and W. Zhang, "A multi-charger cooperative energy provision algorithm based on density clustering in the industrial Internet of Things," *IEEE Internet Things J.*, to be published. doi: 10.1109/JIOT.2019.2928557.

[11] L. Liu, G. Han, Y. He, and J. Jiang, "Fault-tolerant event region detection on trajectory pattern extraction for industrial wireless sensor networks," *IEEE Trans. Ind. Informat.*, to be published. doi: 10.1109/TII.2019.2933238.

[12] H. Boyes, B. Hallaq, J. Cunningham, and T. Watson, "The industrial Internet of Things (IIoT): An analysis framework," *Comput. Ind.*, vol. 101, pp. 1–12, Oct. 2018.

[13] M. Ali, S. U. Khan, and A. V. Vasilakos, "Security in cloud computing: Opportunities and challenges," *Inf. Sci.*, vol. 305, pp. 357–383, Jun. 2015.

[14] A. Al-Fuqaha, M. Guizani, M. Mohammadi, M. Aledhari, and M. Ayyash, "Internet of Things: A survey on enabling technologies, protocols, and applications," *IEEE Commun. Surveys Tuts.*, vol. 17, no. 4, pp. 2347–2376, Nov. 2015.

[15] C. Lin, Y. Bi, H. Zhao, Z. Liu, S. Jia, and J. Zhu, "DTE-SDN: A dynamic traffic engineering engine for delay-sensitive transfer," *IEEE Internet Things J.*, vol. 5, no. 6, pp. 5240–5253, Dec. 2018.

[16] C. Lin, Y. Bi, G. Han, J. Yang, H. Zhao, and Z. Liu, "Scheduling for Time-Constrained Big-File Transfer over Multiple Paths in Cloud Computing," *IEEE Trans. Emerg. Topics Comput. Intell.*, vol. 2, no. 1, pp. 25–40, Jan. 2018.

[17] S. Schneider, "The industrial Internet of Things (IIoT): Applications and taxonomy," in *Internet of Things and Data Analytics Handbook*, vol. 10, no. 2. Hoboken, NJ, USA: Wiley, Feb. 2017, pp. 41–81.

[18] R. D. Matthews, J. E. Peters, S. A. Beckel, and M. Shizhi, "A new technique for thermodynamic engine modeling," *Energy*, vol. 7, no. 6, pp. 667–675, Nov./Dec. 1983.

[19] D. L. Volponi and D. L. Simon, "Enhanced self tuning on-board real-time model (eSTORM) for aircraft engine performance health tracking," *Inf. Sci.*, vol. 305, no. 6, pp. 79–90, Jul. 2015.

[20] C. Maes and A. Salazar, "Linear response in the nonequilibrium zero range process," *Chaos, Solitons Fractals*, vol. 64, no. 1, pp. 78–87, Jul. 2014.

[21] A. Doerr, C. Daniel, D. Nguyen-Tuong, A. Marco, S. Schaal, T. Marc, and S. Trimpe, "Optimizing long-term predictions for model-based policy search," in *Proc. 1st Annu. Conf. Robot Learn.*, Mountain View, CA, USA, Nov. 2017, vol. 78, no. 1, pp. 227–238.

[22] C. Cai, L. Fan, and B. Wu, "Numerical simulation of combustor temperature performance of a high-temperature high-speed heat-airflow simulation system," *World J. Eng.*, vol. 13, no. 5, pp. 422–431, Oct. 2016.

[23] H. Li, G. Gao, R. Chen, X. Ge, S. Guo, and L.-Y. Hao, "The influence ranking for testers in bug tracking systems," *Int. J. Softw. Eng. Knowl. Eng.*, vol. 29, no. 1, pp. 93–113, Sep. 2019.

[24] B. Wang, X. Wang, Y. L. Shi, and H.-W. Wang, "A real-time piecewise linear dynamic model of aeroengine," *J. Aerosp. Power*, vol. 29, no. 3, pp. 696–701, Mar. 2014.

[25] Z. Tang, "On study of application of big data and cloud computing technology in smart campus," in *Proc. IOP Conf., Earth Environ. Sci.*, Dec. 2017, vol. 100, no. 1, Art. no. 012026.

[26] J. Popelka and P. Starý, "Mathematical model of a turbocharged engine," *Appl. Mech. Mater.*, vols. 799–800, pp. 842–846, Oct. 2015.

[27] C. Lu, H. Liu, D. Song, X. Yang, Q. Tan, X. Hu, and X. Kang, "The establishment of LTO emission inventory of civil aviation airports based on big data," in *Proc. IOP Conf., Earth Environ. Sci.*, Mar. 2018, vol. 128, no. 1, Art. no. 012069.

[28] Y. X. Guo, Y. J. Chao, Z. H. Gan, S. Z. Li, and B. Wang, "Performance analysis on free-piston stirling cryocooler based on an idealized mathematical model," in *Proc. IOP Conf., Mater. Sci. Eng.*, Dec. 2017, vol. 278, no. 1, Art. no. 012174.

[29] Z. Dong, J.-Z. Lu, L. Wang, and J. Li, "Research of model-based aero-engine control system design structure and workflow," *Procedia Eng.*, vol. 99, no. 603, pp. 788–794, Dec. 2015.

[30] B. Yu, C. Cao, W. Shu, and Z. Hu, "A new method for the design of optimal control in the transient state of a gas turbine engine," *IEEE Access*, vol. 5, pp. 23848–23857, 2017.
[31] W. Dong, P. Shao, W. Xie, Y. Lin, and X. Sun, "Dynamic surface control design for the rotating stall and surge in an aeroengine compressor," *Asian J. Control*, vol. 17, no. 5, pp. 2025–2032, Sep. 2015.
[32] A. Biondi, M. D. Natale, and G. Buttazzo, "Response-time analysis for real-time tasks in engine control applications," in *Proc. Acm/IEEE 6th Int. Conf. Cyber-Phys. Syst.*, Vienna, Austria, Apr. 2015, pp. 120–129.
[33] H. Karabulut, C.Çınar, E. Oztürk, and H. S. Yücesu, "Torque and power characteristics of a helium charged stirling engine with a lever controlled displacer driving mechanism," *Renew. Energy*, vol. 35, no. 1, pp. 138–143, Jan. 2010.
[34] Y. Wang, L. I. Qiu-Hong, and X. H. Huang, "Research of variable cycle engine modeling techniques," *J. Aerosp. Power*, vol. 28, no. 4, pp. 954–960, Apr. 2013.
[35] G. Y. Chung and J. V. R. Prasad, "Turbofan engine transient response predictions using real-time analytical linear models," in *Proc. 50th AIAA/ASME/SAE/ASEE Joint Propuls. Conf.*, Cleveland, OH, USA, Jul. 2014, pp. 3926–3932.
[36] S. Yang, X. Wang, Y.-F. Long, Z.-P. Li, Z. Hu, K. Yin, and R. Zhang, "Partition method for improvement of piecewise linear model with full envelope covered," *J. Aerosp. Power*, vol. 28, no. 4, pp. 954–960, Apr. 2013.
[37] Y. Yang, G. Zhang, and S.-C. Chen, "The application of Taylor series expansion in physical chemistry," *Daxue Huaxue*, vol. 32, no. 7, pp. 83–87, Jul. 2017.
[38] S. N. Maceachern and S. Guha, "Parametric and semiparametric hypotheses in the linear model," *Can. J. Statist.*, vol. 39, no. 1, pp. 165–180, Mar. 2015.
[39] V. R. Katta and W. M. Roquemore, "Numerical method for simulating fluid-dynamic and heat-transfer changes in jet-engine injector feed-arm due to fouling," *J. Thermophys. Heat Transf.*, vol. 7, no. 4, pp. 651–660, Oct. 1993.
[40] H. Wu, H. Jia, and W. Feng, "Exploring effects of fuel scheduling on start-up process of augmented turbofan engine," *J. Northwestern Polytech. Univ.*, vol. 28, no. 1, pp. 113–117, Jan. 2010.
[41] S. Zhang, F. Liao, Y. Chen, and K. He, "Aircraft trajectory control with feedback linearization for general nonlinear system," Dec. 2017, *arXiv:1712.10077*. [Online]. Available: https://arxiv.org/abs/1712.10077
[42] S. Sahu, D. N. Asthana, D. Chaturvedi, and K. B. Sahay, "An improved method for mppt for wind solutions using newton raphson technique with stability analysis of the optimal power curve," in *Proc. 21st Century Energy Needs-Mater., Syst. Appl. (ICTFCEN)*, Kharagpur, India, Nov. 2016, pp. 1–6.
[43] J. Lu, Y.-Q. Guo, and X.-L. Chen, "Establishment of aero-engine state variable model based on linear fitting method," *J. Aerosp. Power*, vol. 26, no. 3, pp. 1172–1177, May 2015.
[44] F. Sun, Y. Du, and H. Zhang, "A study on optimal control of the aero-propulsion system acceleration process under the supersonic state," *Chin. J. Aeronaut.*, vol. 30, no. 2, pp. 698–705, Apr. 2017.
[45] J. W. Chapman, T. M. Lavelle, J. S. Litt, and T.-H. Guo, "A process for the creation of T-MATS propulsion system models from NPSS data," in *Proc. 50th AIAA/ASME/SAE/ASEE Joint Propuls. Conf.*, Cleveland, OH, USA, Jan. 2014, pp. 3931–3939.
[46] S. Ioffe and C. Szegedy, "Batch normalization: Accelerating deep network training by reducing internal covariate shift," in *Proc. Int. Conf. Mach. Learn.*, Jul. 2015, pp. 448–456.

LINFENG GOU received the Ph.D. degree from Northwestern Polytechnical University, in 2010, where he is currently an Associate Professor of power control engineering and the Vice President with the Power and Energy College. He has participated in many national key projects. His main research interests include fault diagnosis and fault tolerant control of aero-engine control systems.

XIANYI ZENG received the B.S. degree in aircraft engineering from the Zhengzhou University of Aeronautics, Zhengzhou, China, in 2018. She is currently pursuing the master's degree with the School of Power and Energy, Northwestern Polytechnical University, Xi'an, China. Her research interests include aero engine modeling and analysis based on the Industrial Internet of Things.

ZHAOHUI WANG received the B.S. degree from the School of Software, Dalian University of Technology, Dalian, China, where he is currently pursuing the master's degree with the School of Software. His research interests include UWSNs, the Industrial IoT, and software defined networking.

GUANGJIE HAN received the Ph.D. degree from Northeastern University, Shenyang, China, in 2004. From 2004 to 2005, he was a Product Manager with ZTE Company. From 2005 to 2006, he was the Key Account Manager with Huawei Company. In February 2008, he was a Postdoctoral Researcher with the Department of Computer Science, Chonnam National University, Gwangju, South Korea. From January 2017 to February 2017, he was a Visiting Professor with the City University of Hong Kong, China. He is currently a Distinguished Professor with the College of Engineering, Nanjing Agricultural University, Nanjing, China, and a Professor with the Dalian University of Technology, Dalian, China. He is the author of more than 330 articles published in related international conference proceedings and journals, including the IEEE COMST, the IEEE TII, the IEEE TMC, the IEEE TVT, the IEEE TIE, the IEEE TPDS, the IEEE TETC, the IEEE IoT Journal, the IEEE TETCI, the IEEE TCC, the IEEE Systems, the IEEE Sensors, the IEEE Wireless Communications, the IEEE Communications, and the IEEE Network. He is the holder of 125 patents.

CHUAN LIN received the B.S. degree in computer science and technology from Liaoning University, Shenyang, China, in 2011, the M.S. degree in computer science and technology from Northeastern University, Shenyang, in 2013, and the Ph.D. degree in computer architecture, in 2018. He was a visiting Ph.D. student with the Network Architecture and Services Group, Delft University of Technology, Delft, The Netherlands, from 2015 to 2017. He is currently a Postdoctoral Researcher with the School of Software, Dalian University of Technology, Dalian, China. His research interests include UWSNs, the Industrial IoT, and software defined networking.

XU CHENG received the B.S. degree from Northwestern Polytechnical University, Xi'an, China, in 2018, where he is currently pursuing the master's degree with the School of Power and Energy. His research interest includes aircraft engine model linearization.